Quantifying the sources of increasing stratospheric water vapour concentrations

Patrick E. Sheese[1], Kaley A. Walker[1], Chris D. Boone[2], and David A. Plummer[3]

[1]University of Toronto, Department of Physics, Toronto, Canada
[2]University of Waterloo, Department of Chemistry, Waterloo, Canada
[3]Candian Centre for Climate Modelling and Analysis, Environment and Climate Change Canada, Montreal, Canada

Correspondence: Kaley A. Walker (kaley.walker@utoronto.ca)

Abstract. According to satellite measurements from multiple instruments, water vapour (H_2O) concentrations, in most regions of the stratosphere, have been increasing at a statistically significant rate of $\sim$1-5% dec^{-1} since the early 2000s. Previous studies have estimated stratospheric H_2O trends, but none have simultaneously quantified the contributions from all main sources (temperature variations in the tropical tropopause region, changes in the Brewer-Dobson circulation, and changes in methane (CH_4) concentrations and oxidation) at all latitudes. Atmospheric Chemistry Experiment – Fourier Transform Spectrometer (ACE-FTS) measurements are used to estimate altitude/latitude-dependent stratospheric H_2O trends from 2004-2021 due to these sources. Results indicate that rising temperatures in the tropical tropopause region play a significant role in the increases, accounting for $\sim$1-4% dec^{-1} in the tropical lower-mid stratosphere, as well as in the mid-latitudes below $\sim$20 km. By regressing to ACE-FTS N_2O concentrations, it is found that in the lower-middle stratosphere, general circulation changes have led to both significant H_2O increases and decreases on the order of 1-2% dec^{-1} depending on altitude/latitude region. Making use of measured and modelled CH_4 concentrations, the increase in H_2O due to CH_4 oxidation is calculated to be $\sim$1-2% dec^{-1} above $\sim$30 km in the Northern Hemisphere and throughout the stratosphere in the Southern Hemisphere. After accounting for these sources, there are still regions of the midlatitude lower-mid stratosphere that exhibit significant residual H_2O trends increasing at 1-2% dec^{-1}. Results indicate that these unaccounted for increases could potentially be explained by increases in upper tropospheric molecular hydrogen.

1 Introduction

Water vapour (H_2O) is the most abundant greenhouse gas in the Earth's atmosphere. Much like other greenhouse gases, it absorbs shortwave radiation near the surface, leading to temperature increases, and emits longwave radiation in the stratosphere and above, leading to upper atmospheric cooling. Near the surface, H_2O is part of a positive feedback loop where increasing temperatures lead to an increase in the saturation vapour pressure, leading to more H_2O in the atmosphere, leading to more heating, and so on. Because H_2O is controlled predominantly by this feedback system in the troposphere, and due to its much shorter atmospheric lifetime (with respect to other greenhouse gases) on the order of weeks near the surface and 10-20 years in the stratosphere (Brasseur and Solomon, 2005), H_2O is typically considered an amplifier of the greenhouse effect rather than a contributor (e.g., Chung et al., 2014). Downward propagating radiation from stratospheric H_2O can also lead to upper

troposheric heating (e.g., Manabe and Wetherald, 1967; de F. Forster and Shine, 1999; Forster and Shine, 2002). It is therefore important to continually monitor and understand H_2O variations throughout the troposphere and stratosphere.

Although the predominant source of stratospheric H_2O is moisture-rich tropospheric air that is lofted upwards in the tropics as part of the Brewer-Dobson circulation (BDC), the physical processes that control the amount of water vapour in the stratosphere are fundamentally different from those in the troposphere. As that moisture-rich tropospheric air crosses the cold tropical tropopause region, it freeze-dries, removing most of the H_2O before entering the stratosphere (Brewer, 1949; Holton and Gettelman, 2001, and references therein). With few other sources, and its relatively long stratospheric lifetime, much of the stratospheric H_2O budget is a function of tropical tropopause cold-point temperature, especially in the lower stratosphere. As such, time series of tropical tropopause region temperatures are often used as a regressor in determining stratospheric H_2O trends (Hegglin et al., 2014, and references therein). Hegglin et al. (2014) showed that variations in low-mid latitude, lower stratospheric H_2O very closely followed variations in modelled mean tropical temperatures at 100 hPa. At higher altitudes and more poleward latitudes, H_2O variations tended to follow those of the modelled temperatures with a lag of a few months (tape recorder effect (Mote et al., 1996)).

Another major source of stratospheric H_2O is CH_4 oxidation via reactions with OH, $O(^1D)$, and Cl. As detailed in Brasseur and Solomon (2005), oxidation of CH_4 via OH can produce H_2O directly, but all three reactions have byproducts that lead to the production of a formaldehyde molecule (CH_2O), which is then quickly destroyed via multiple reactions that can produce H_2O molecules. In the stratosphere, on average, an oxidized CH_4 molecule produces ~2 H_2O molecules, however that average varies with altitude and latitude (e.g., Jones et al., 1986; le Texier et al., 1988; Frank et al., 2018).

A minor source of stratospheric H_2O is the oxidation of H_2, which can be an indirect product of CH_4 oxidation or transported into the stratosphere from the tropical troposphere. Both Wrotny et al. (2010) and Frank et al. (2018) have shown that it is possible for the ratio of H_2O production to CH_4 loss, α, in the tropical stratosphere to be greater than 2. Wrotny et al. (2010) used satellite measurements from HALOE (Halogen Occultation Experiment), ACE-FTS (Atmospheric Chemistry Experiment – Fourier Transform Spectrometer), and MIPAS (Michelson Interferometer for Passive Atmospheric Sounding) to show that α can be on the order of 2.0-3.7, attributing the additional production to oxidation of H_2 that was not produced via CH_4 oxidation.

A number of studies have recently been conducted that have measured stratospheric H_2O increases from satellite measurements, however, none of them parse trends in order to determine the relative contributions from each of the three main sources throughout the stratosphere. For instance, similar to Hegglin et al. (2014) and Tao et al. (2023), Randel and Park (2019) used merged HALOE and Aura/MLS (Microwave Limb Sounder) data to show that the majority of variations in lower stratospheric H_2O from 1993-2017 can be explained by changes in tropical cold point temperature. Yue et al. (2019) determined that both SABER (Sounding of the Atmosphere using Broadband Radiometry) and Aura/MLS measurements exhibited stratospheric H_2O trends on the order of 5-6% dec^{-1} since the early 2000's. As to the sources of those increases, they determined that the H_2O trends in the lower stratosphere are consistent with frost-point hygrometer measurements, and mesospheric trends are much greater than what is expected assuming complete CH_4 oxidation. Similarly, Fernando et al. (2020) found that profiles of global ACE-FTS, Aura/MLS, and SABER H_2O trends agreed well, but could not be explained solely by CH_4 oxidation. ACE-FTS is in a unique position when it comes to investigating the influence of CH_4 oxidation on stratospheric H_2O trends as

60 <u>it is currently the only Earth observing satellite instrument that makes vertically resolved measurements of both H_2O and CH_4 throughout the stratosphere.</u>

This study uses simultaneously-measured profiles of H_2O, CH_4, and N_2O from ACE-FTS (a measurement combination that only ACE-FTS is currently producing) in order to measure height resolved H_2O trends throughout the stratosphere in latitudinal bands spanning 80°S-80°N. The sources of those trends are then quantified, considering contributions due to temperature

65 changes in the tropical tropopause region, structural changes in the BDC, and changes in local and tropical tropopause region CH_4 concentrations.

A description of the satellite measurements used in this study can be found in Section 2, and the methodology is described in Section 3. The ACE-FTS H_2O trends and the contributions from different sources are discussed in Section 4, and all the results are summarized in Section 5.

70 ## 2 ACE-FTS on SciSat

The ACE-FTS instrument (Bernath et al., 2005) is one of two instruments on board the Canadian SciSat satellite, which was launched into a high inclination orbit in August 2003. Starting in February 2004, ACE-FTS began measuring profiles of temperature, pressure, and concentrations of multiple atmospheric trace species, including H_2O, CH_4, and N_2O. The instrument is a high-spectral-resolution (0.02 cm^{-1}) spectrometer viewing the Earth's limb in the infrared between 750 and 4400 cm^{-1},

75 using solar occultation viewing geometry. The vertical profiles span 5-150 km with a vertical spacing of $\sim$2 to 6 km, depending on the orbital geometry, and the circular field-of-view at the tangent altitude is on the order of 3-4 km. This study makes use of the most recent version of level 2 data, version 5.2 (v5.2), which provides interpolated data on a 1-km grid. The retrieval algorithm, described by Boone et al. (2005, 2013, 2020, 2023) uses a non-linear, least-squares, global-fitting technique that fits observed atmospheric transmission spectra to forward modelled spectra in species/altitude dependent microwindows. The

80 modelled spectra are calculated using spectral line parameters from the HITRAN2020 database (Gordon et al., 2022). In all retrievals, horizontal homogeneity is assumed and diurnal variations are not taken into account along the line-of-sight.

Version 5.2 of the H_2O retrievals makes use of 63 microwindows between 937 and 3173 cm^{-1}, has altitude limits of 5 and 95 km, and in the stratosphere accounts for CO_2, O_3, N_2O, CH_4, NO_2, HNO_3, NO, and COF_2, as well as isotopologues H_2O, CO_2, N_2O, and CH_4 as interfering species. ACE-FTS H_2O has been used in over 50 different studies, including the European

85 Space Agency's Water Vapour Climate Change Initiative (Hegglin and Ye, 2022; Ye et al., 2022), merged data studies (e.g., Froidevaux et al., 2015; Davis et al., 2016), and multiple validation studies (e.g., Wetzel et al., 2013; Weaver et al., 2019; Rong et al., 2019). Fernando et al. (2020) examined ACE-FTS v4.0 H_2O and CH_4 trends in the stratosphere and mesosphere, however focused on 55°S-55°N mean values. Although the study did not quantify the different sources contributing to H_2O trends, it was concluded that increasing CH_4 trends were not sufficient to fully explain the observed increases in stratospheric

90 H_2O.

The latitudinal coverage of the instrument is shown in Fig.1. As can be seen, the annually-repeating measurements are made predominantly in the high latitudes, with the tropics being sampled roughly every three months. However, significant trends are still capable of being detected at the lower latitudes due to the long lifetime of the ACE-FTS data sets.

3   Methodology

Many different trends are calculated in this study, each of them making use of the multiple linear regression (MLR) technique (Chatterjee and Hadi, 1986), using various predictor data sets (in different combinations) as regressors. In each case; whether it is ACE-FTS H_2O, CH_4, or N_2O trends; the time series are fit to a model of the form,

$$y_{fit} = \beta_0 + \beta_1 l(t) + \sum_i \beta_i r_i(t), \tag{1}$$

where t is time in years, β are the fit components, $l(t)$ is a linear function increasing from -0.5 to 0.5 over the length of the time series being fitted, and $r(t)$ are the considered regressor time series. The regressor time series used in this study are,

- two annual oscillation terms $\cos 2\pi t$ and $\sin 2\pi t$ (AO) and two semi-annual oscillation terms $\cos 4\pi t$ and $\sin 4\pi t$(SAO), with t measured in years;

- monthly mean tropical tropopause region temperatures from ECMWF (European Centre for Medium-Range Weather Forecasts) Reanalysis version 5 (ERA5 (Hersbach et al., 2020)) data (as described below);

- simultaneously measured ACE-FTS N_2O data as a proxy for dynamical processes (Dubé et al., 2023). As per Dubé et al. (2023), local N_2O time series at all altitudes and latitudes have a 2.8% dec^{-1} trend (corresponding to the 2004-2022 global surface N_2O trend) removed prior to being used as a regressor;

- daily mean F10.7 cm solar radio flux values (which indirectly affect H_2O concentrations via influences on O_3 and temperature) provided by Geomagnetic Observatory Niemegk, Potsdam (Matzka et al., 2021);

- monthly mean Quasi-Biennial Oscillation (QBO) proxies of the 30 and 50 hPa Singapore zonal winds (Baldwin et al., 2001, obtained from https://www.geo.fu-berlin.de/en/met/ag/strat/produkte/qbo/index.html, last access: 30 Sept 2023));

- monthly mean El Niño/Southern Oscillation (ENSO) index values from the NOAA Physical Sciences Laboratory (Wolter and Timlin, 2011, obtained from https://psl.noaa.gov/enso/mei/, last access 30 Sept 2023);

- monthly mean tropopause pressure (trop) values from NCEP-NCAR reanalysis data (Kalnay et al., 1996, obtained from ftp://cdc.noaa.gov/, last access 10 Jan 2025).

H_2O trends were calculated at all ACE-FTS altitudes (1-km grid) between 17.5 and 55.5 km—roughly between the hygropause and stratopause—in sixteen $10°$ bins between $80°$S and $80°$N, for daily-mean time series. To avoid influences from measurements within and near the polar vortexes, scaled potential vorticity (sPV) values derived from the Modern Era Retrospective

4

analysis for Research and Applications, Version 2 (MERRA-2 (Gelaro et al., 2017)) interpolated to ACE-FTS locations (Manney et al., 2007) were employed. Only data with a corresponding absolute sPV value of 1.4×10^{-4} s^{-1} or less were used in this study.

In order to fit to tropical tropopause region temperatures, a time series of monthly mean temperatures within 15°S-15°N at 100 hPa for years 1988-2022 was obtained from ERA5 data (shown in Fig. 2). In the tropical lower stratosphere, it is expected that the H$_2$O time series would closely follow the ERA5 temperature time series. However, at locations further from the tropical lower stratosphere, the H$_2$O response is expected to be lagged with respect to the temperature time series, as it takes longer for air entering the stratosphere to reach those locations, as discussed above. In the fitting algorithm, at each altitude and latitude bin, the regression was performed with the ERA5 temperatures lagged by 0-15 years in 2-day increments to find the lag time that minimized the residual between the ACE-FTS H$_2$O data and the MLR fit. Only lag times that led to a positive correlation between the H$_2$O and temperature time series were considered, and the lagged temperature time series will be referred to hereafter as T_{lag}. At the lowest altitude level in the 0-10°S and 0-10°N latitude bins, lag times were restricted to within 2 months, and lag times at any other given altitude/latitude bin were restricted to a value within ±24 months of adjacent bins. Although the ERA5 time series was lagged by up to 15 years in each altitude/latitude bin, it was found that the maximum lag time required to minimize the residuals in any bin was 60 months, whereas stratospheric mean age-of-air estimates tend to be on the order of 0-15 years, depending on altitude and latitude. This can be explained by the fact that lagging the temperature time series assumes that the measured air parcel is a singular parcel that traveled from the entry point to the measurement location with a particular transit time and does not account for mixing or changes in transit pathways (Poshyvailo-Strube et al., 2022).

To ensure that it is appropriate to simultaneously use T_{lag} and local N$_2$O time series as regressors, the correlation between these time series was calculated in each altitude and latitude bin. At all altitudes and latitudes, the absolute correlation between measured N$_2$O and T_{lag} time series is less than 0.35 and is typically below 0.2. The same is true for the correlation between N$_2$O and the seasonal cycles, and for T_{lag} and SAO–although between T_{lag} and SAO the correlation is typically on the order of 0.2-0.3. T_{lag} and AO, however, are not independent as the tropopause region temperatures exhibit a significant annual oscillation. The implications of this are discussed in Sect. 4.2.

Although CH$_4$ oxidation is a major source of stratospheric H$_2$O, ACE-FTS measurements of local CH$_4$ concentrations are not an appropriate regressor, as local H$_2$O concentrations depend on the amount of CH$_4$ that has been oxidized in the air parcel since entering the stratosphere, which is a function of the difference between the CH$_4$ concentration at time of entry and the local CH$_4$ concentration,

$$[H_2O]_{CH_4} = \alpha[CH_4]_{oxidized} = \alpha([CH_4]_{entry} - [CH_4]_{local}), \tag{2}$$

where α is the H$_2$O yield from oxidized CH$_4$. In past studies, α is often assumed to be a constant of 2 throughout the stratosphere (e.g., Stowasser et al., 1999; Myhre et al., 2007; Frank et al., 2018). However, Frank et al. (2018) showed that this assumption tends to overestimate H$_2$O production in the lower stratosphere and underestimate H$_2$O production nearer the stratopause. In this study, a height dependent α is used based on the global effective H$_2$O yield profile shown in Fig. 14 of

Frank et al. (2018), which is ∼1.6 in the lower stratosphere and ∼2.2 at the stratopause. To account for the fraction of H_2O trends due to CH_4 oxidation, the time derivative of Eq. 2 is taken,

155
$$\frac{d[H_2O]_{CH_4}}{dt} = \alpha\left(\frac{d[CH_4]_{entry}}{dt} - \frac{d[CH_4]_{local}}{dt}\right).$$
(3)

The local CH_4 trends are determined by regressing to ACE-FTS N_2O data (in addition to AO and SAO time series) to account for changes in CH_4 due to changes in the general circulation,

$$\frac{d[CH_4]_{local}}{dt} = \beta_0 + \beta_1 l(t) + \beta_{AO}^{(2)} AO + \beta_{SAO}^{(2)} SAO + \beta_{N_2O}[N_2O].$$
(4)

Since ACE-FTS has low sampling in the tropical region, model data from the specified dynamics run of the Canadian
160 Middle Atmosphere Model (CMAM39-SD) (Beagley et al., 1997; Scinocca et al., 2008; McLandress et al., 2014) were used to supplement the ACE-FTS data when calculating CH_4 entry trends. The CMAM39-SD run (referred to as CMAM39 hereafter) spans 1979-2018 inclusive, with simulations relaxed towards six-hourly fields of temperature, vorticity, and divergence from ERA-Interim (Dee et al., 2011) reanalysis data. The chemical forcing fields for long-lived greenhouse gases, including CH_4, were obtained from the Coupled Model Intercomparison Project Phase 6 (CMIP6) (Eyring et al., 2016)) historical time series
165 (Meinshausen et al., 2017) up to 2014, and the SSP2-4.5 scenario (Meinshausen et al., 2020) for the remaining years. They were forced as a time-dependent mixing ratio specified for the bottom two model layers (approximately 100 m in depth) based on the global and annual average mixing ratio taken as the mid-year value and linearly interpolated in time to provide values at intermediate times.

The mean of the ACE-FTS 15°S-15°N, 100-200 hPa, 180-day running zonal mean and the CMAM39 15°S-15°N, 100-
170 200 hPa, daily zonal mean was calculated, shown in Fig. 2. This ACE-CMAM mean time series (black dashed line in Fig. 2) was used to determine a CH_4 entry trend of 78±1 ppbv/dec between 2004 and 2022. The uncertainties for $\frac{d[CH_4]_{entry}}{dt}$ and $\frac{d[CH_4]_{local}}{dt}$ are added together in quadrature, as are the uncertainties in $\frac{d[H_2O]_{CH_4}}{dt}$ and the fitted H_2O trend uncertainties (all uncertainties are the statistical uncertainties of the calculated trends, excluding measurement uncertainties, which are assumed to be negligible). This method however assumes that CH_4 trends at the stratospheric entry point have been constant from
175 the time of entry to the time period for which the local CH_4 trends are being calculated, which could be a difference of up to the order of a decade. As seen in the CMAM CH_4 time series, and as discussed by, e.g., Dlugokencky et al. (2003) and Rigby et al. (2008), there was a slowdown in the increase of CH_4 concentrations just before the beginning of the ACE mission (∼1999-2003) just below the tropical tropopause. This affect is accounted for and discussed when examining H_2O trends using time-lagged CH_4 entry trends in Sect. 4.2.
180 All ACE-FTS data were screened for outliers using data quality flags, as per Sheese et al. (2015), prior to analysis. At all altitude levels used in this study, the screening rejects less than 1% of the data. Only data prior to 2022 were used as to avoid any influence from H_2O injected by the Honga Tonga-Honga Ha'apai eruption in January 2022.

4 Results

The following sections discuss results of MLR trend analysis on the ACE-FTS H_2O time series using different regressors. The "full" H_2O trends are those where only the AO and SAO time series (that do not themselves have any trend) are used as regressors. Results are also shown for H_2O "residual" trends, which are the resulting trends when using additional time series that may contain a trend as regressors. The differences between the full trends and the residual trends (labelled as Δ in figure panels) are considered to be the contribution to the full trend due to the regressors used in the analysis.

Section 4.1 discusses the full H_2O trends as well as the individual contributions to the full H_2O trends due to solar flux, QBO, and ENSO influences; structural BDC changes; and changes in tropical tropopause region temperatures. Section 4.2 analyzes the contribution to the full H_2O trends due to CH_4 oxidation under two different assumptions: first, simply assuming a constant $\frac{d[CH_4]_{entry}}{dt}$ over the past few decades and then accounting for the fact that $\frac{d[CH_4]_{entry}}{dt}$ has not been constant and allowing the value used to vary depending on altitude and latitude. The discussion then focuses on the remaining residual trends, which can still be statistically significant, after all the above-mentioned individual sources contributing to the full trends are accounted for.

4.1 Standard MLR Results

A simple MLR analysis of the ACE-FTS H_2O trends, regressing only to ~~linear components and~~ annual and semi-annual cycles, are shown in the left panel of 3 and the corresponding trend uncertainties (95% confidence level) are shown in the right panel. The results clearly show that since 2004 stratospheric H_2O has been increasing, or has had no significant trend, throughout the stratosphere. There is a noted hemispheric asymmetry at all altitudes, except for around the highest altitudes, $\sim$50-55 km, where trends are on the order of 2-3%. In the Southern Hemisphere (SH), H_2O trends also tend to be on the order of 2-3%, except near the tropical lower stratosphere. In the Northern Hemisphere (NH), H_2O trends tend to be somewhat more variable, with values of 3-5% dec^{-1} up to $\sim$30 km and $\sim$1-3% dec^{-1} above 30 km.

The left panel of Fig. 4 again shows the trend results from a simple MLR analysis of the ACE-FTS H_2O time series, regressing only to ~~linear components and~~ annual and semi-annual cycles, and these are shown to compare to the residual H_2O trends when regressing to the F10.7 cm, QBO, ENSO, and trop time series, shown in the middle panel. The differences in the H_2O trend values are typically less than $\pm$0.5% dec^{-1} in all altitude/latitude bins (except within 70-80°S), and the differences due to F10.7 cm alone are typically only within $\pm$0.2% dec^{-1} (not shown).

The effects of ~~ENSO conditions~~ time-lagging ENSO and tropopause pressure ~~on stratospheric H_2O, however, are not instantaneous. Similar to the time-lagging method described in Sect. 3, the ENSO and trop time series were lagged to find lag times in each bin that maximize the correlations between local H_2O and the respective index time series. The influence of lagged ENSO and lagged trop on H_2O trends are shown in the top panel of Fig. A1 and the respective corresponding optimal lag times in months are shown on the bottom. The influence of both lagged ENSO and lagged trop is still typically less than 1% dec^{-1} throughout the stratosphere.~~ are discussed in Appendix A1.

215   In all following analyses, QBO, ENSO, and trop indicies are not used in the regression schemes as the effects they are meant to represent can also be accounted for by the ACE-FTS N_2O time series.

    As shown in Dubé et al. (2023), simultaneous measurements of N_2O, a long-lived atmospheric tracer, can be used as a proxy for changes in the BDC and can be used as an alternate regressor to account for trends due to dynamical processes in the stratosphere. The middle panel of Fig. 5 shows the residual H_2O trends after regressing to local ACE-FTS N_2O, and the

220 right panel shows the difference between the full H_2O trend and those after regressing with N_2O. The remaining trends are all increasing (Fig. 5, middle panel) but the hemispheric asymmetry in the lower stratosphere flips sign and the remaining trends are more strongly positive in the SH ($\sim$3% dec^{-1}) compared to the NH (1-3% dec^{-1}). Above $\sim$35 km the remaining H_2O trends are more consistent between hemispheres, on the order of 1-3% dec^{-1}. These results are consistent with those of Tao et al. (2023). The differences (right panel of Fig. 5) represent the trend in H_2O due to changes in the general circulation, showing

225 that the net hemispheric asymmetry in H_2O trends can be attributed to changes in stratospheric circulation. In particular, the influence can be to either increase or decrease local H_2O concentrations, depending on the region. Changes in the BDC account for an increase in H_2O of 1-2% dec^{-1} in the NH near 20-30 km and a decrease in H_2O of 1-2% dec^{-1} in the NH near 30-40 km as well as in the SH near 25-30 km. In all other regions, the contribution of dynamical processes to H_2O trends is not statistically significant.

230   Climate models have long indicated that increasing concentrations of greenhouse gases in the lower atmosphere should lead to an acceleration of both the shallow and deep branches of the BDC (e.g., Butchart, 2014, and references therein). Multiple studies have examined measurements of atmospheric proxies for BDC changes and have detected accelerations in the shallow branch (below 20 km), although not at higher altitudes in the deep branch (e.g., Engel et al., 2009; Diallo et al., 2012; Engel et al., 2017). However, recent studies have suggested that decreasing concentrations of ozone depleting substances in the

235 stratosphere can lead to a deceleration of the BDC (e.g., Polvani et al., 2018; Fu et al., 2019). Polvani et al. (2018) analyzed data from WACCM runs for 1965-2080 and showed that between 2000 and 2080, the BDC is expected to slow down due to the removal of ozone depleting substances. Fu et al. (2019) show that within 2000-2018 there has been a slowing down of the BDC in the SH lower stratosphere (10-50 hPa), but no clear overall trend in the NH. This agrees with ACE-FTS showing a decrease in H_2O due to structural circulation changes throughout most of the SH and a combination of increasing and decreasing

240 circulation in the NH depending on the season. Since Fu et al. (2019) averaged data over the entire NH from 10-50 hPa, it is unknown whether the spatial patterns of the seasonal differences they reported would be in agreement with the BDC results in this study.

    Since it can take months to years for newly introduced stratospheric air (in the tropical lower stratosphere) to be transported throughout the stratosphere, including time-lagged ERA5 tropical upper-tropospheric temperatures (T_{lag}) in the regression has

245 a significant effect on the trend results. Including T_{lag} in the regression can decrease the residual trends by up to 4% dec^{-1}, as seen in Fig. 6, indicating a warming trend near the tropical tropopause, which would allow more H_2O to enter the stratosphere. In the tropics, this warming is contributing a $\sim$2-4% dec^{-1} increase in H_2O below 20 km, and a $\sim$1-2% increase in the mid stratosphere up to about 45 km (corresponding to a reduction of the residual H_2O trends). The warming also contributes a 1-3% increase in H_2O in the mid-latitude lower stratosphere (below $\sim$20 km). Elsewhere, including T_{lag} as a regressor does

250 not significantly affect H_2O trends, with differences from the full trend typically within $\pm 1\%$. Figure 7 shows the lag times that were determined to minimize the difference between the fit and the ACE-FTS data. As expected, the lag times increase with altitude and with absolute latitude, as stratospheric age of air increases. The lag times are on the order of a 1-2 months near the equator in the lower stratosphere and increase up to 3-5 years nearer the high-latitude stratopause regions.

4.2 Accounting for CH_4 oxidation

255 In order to quantify how much CH_4 oxidation is contributing to stratospheric H_2O trends, first local ACE-FTS CH_4 trends were calculated using an annual cycle, a semi-annual cycle, and ACE-FTS N_2O time series as regressors. As seen in the left panel of Fig. 8, the CH_4 trends are increasing in all regions and also exhibit a significant hemispheric asymmetry. In the mid-high latitudes, NH CH_4 trends range from 3% dec^{-1} in the lower stratosphere up to 12% dec^{-1} near 55 km. These trends are greater than the SH trends that increase from 2% dec^{-1} up to 8% dec^{-1}. At the lower latitudes, hemispherical differences are only on
260 the order of 1-2% dec^{-1}, with relatively larger trends in the NH around 20-30 km and relatively larger trends in the SH around 40-55 km. The right panel of Fig. 8 shows how those trends contribute to the stratospheric H_2O via Eq. 3. The increases in CH_4 concentrations are leading to an increase of the H_2O budget of $\sim$1-3% dec^{-1} above $\sim$35 km, $\sim$1-2% dec^{-1} below 35 km, with insignificant influence closer to the tropical tropopause region where there is expected to be little to no contribution from methane oxidation.

265 As shown in Fig. 9, when $[H_2O]_{CH_4}$ trends are subtracted from the residual H_2O trends that are calculated regressing to AO, SAO, N_2O, T_{lag}, and F10.7 cm time series, most of the trends throughout the stratosphere are within $\sim \pm 1\%$ dec^{-1} and are not statistically significant. This indicates that these regressors can account for the full ACE-FTS H_2O trends throughout the majority of the stratosphere. The exceptions are in the mid to high latitude regions ($\sim$30-70°S and 40-70°N) in the lower-mid stratosphere ($\sim$20-35 km). In these regions there are still significant residual H_2O trends of $\sim$1-2% dec^{-1}. However,
270 $\frac{d[CH_4]_{entry}}{dt}$ has not been constant over the past 20-30 years, as shown in Fig. 2. To account for this, a time-dependent trend analysis was performed on the CH_4 entry time series. Lagged 18-year trend values for the CMAM-ACE CH_4 entry time series were calculated for lag times of 0-10 years in 5-day intervals (i.e., a lag value of 10 years corresponds to the trend for 1994-2012). The calculated trends versus lag times are shown in Fig. 10, and, as can be observed in Fig. 2, the 18-year CH_4 entry trends have been increasing since the early 1990's. This method of using lagged $\frac{d[CH_4]_{entry}}{dt}$ was employed by Hegglin et al.
275 (2014). That study used time-lagged $\frac{d[CH_4]_{entry}}{dt}$ with lag times corresponding to the local mean age-of-air. However, ACE-FTS does not have validated measurements of age-of-air throughout the stratosphere, and therefore the optimal lag times from the temperature regression (Fig. 7) are used as a proxy for mean age-of-air.

As expected, the H_2O trends due to CH_4 trends that account for time lags (Fig. 11) are less than those that use a constant CH_4 entry trend value (Fig. 8, right panel). Throughout the stratosphere the CH_4 oxidation contribution leads to a $\sim$0.5-1.5% dec^{-1}
280 increase in H_2O, the larger of those trends tending to be throughout the SH and above $\sim$30 km in the NH.

In each altitude/latitude bin, the CH_4 oxidation contribution was determined using the lagged $\frac{d[CH_4]_{entry}}{dt}$ value that corresponds to that bin's lag time determined for T_{lag} (Fig. 7). The CH_4 oxidation contribution was then subtracted from that bin's residual H_2O trend that used AO, SAO, F10.7 cm, ACE-FTS N_2O, and T_{lag} time series as regressors. The final trend results for

this method are shown in Fig. 12, and it can be seen from the middle panel that when accounting for the non-linear increase in CH$_4$ there are more regions of the stratosphere where there are significant residual H$_2$O trends (than when assuming a constant increase). In the roughly 30-70°S, 20-35 km region, there remains a significant residual H$_2$O trend of 1.0-2.5% dec^{-1}. The residual trend is smaller in the same altitude/latitude region in the NH, between 0.9 and 1.7% dec^{-1}, although near 60°N the region of significant trend extends from up to 55 km. There is also a significant increase of ∼1% dec^{-1} in parts of the SH low-latitude region above 45 km. These results indicate that there is at least one additional source of increasing H$_2$O in multiple regions within the stratosphere that has not been accounted for. It is likely that the regions with unaccounted for trends are actually larger because, as discussed in Sect. 3 the lag times used to determine $\frac{d[CH_4]_{entry}}{dt}$ values only account for transit times from the entry point and does not account for mixing or differences in transit pathways (Poshyvailo-Strube et al., 2022).

~~When accounting for CH$_4$ oxidation with time-lagged entry trends and regressing to~~ The effects on the regression results due to any correlation between the AO components and T_{lag} ~~and N~~or N$_2$O ~~and SAO and no AO components, the resulting residual trends are not meaningfully different below ∼42 km from the same case with AO as a regressor, as seen in Fig. A2. The main differences are above 42 km. Without including AO, the region with significant residual trends in the low-mid latitudes is larger, but still on the order of 1% dec−1, the SH high latitudes exhibit negative residual trends on the order of -1% dec^{-1}, and the NH mid-high latitudes exhibit no significant trends. Therefore, further study is still needed to fully parse the H$_2$O trends in the upper stratosphere~~are discussed in Appendix A2.

As previously mentioned, Wrotny et al. (2010) determined that measurements are consistent with α having a value of up to 3.7 that could account for H$_2$O production via oxidation of H$_2$. Therefore, the H$_2$O trend calculation was done again using the same regressors (AO, SAO, N$_2$O, T_{lag}, F10.7 cm) and the time-lagged CH$_4$ entry trends, but using a constant value of $\alpha = 3.7$ at all altitudes and latitudes. The results of the residual H$_2$O trends are shown in Fig. 13 and are not statistically significant in nearly every bin. It should be noted that the value of α is not being changed in order to "optimize" the results, an extreme acceptable value was used simply to determine what effect that value would have on the calculated H$_2$O trends. Although it is unlikely that the maximum value of $\alpha = 3.7$ is appropriate for all altitudes and latitudes, these results indicate that this higher value of α could be consistent with the calculated ACE-FTS H$_2$O trends, especially in the mid-stratospheric extra-tropics, with the additional production due to increasing tropical tropospheric H$_2$ concentrations. In order to inform further analysis, a model study should be conducted investigating how H$_2$ concentrations have been changing over the course of the ACE-FTS mission lifetime.

One other source of stratospheric H$_2$O that has not been accounted for is convective moistening. In the troposphere, deep convection systems can transport ice particles into the tropopause region and overshooting cloud tops can directly inject water vapour and ice into the lower stratosphere. Recent model studies (e.g., Dauhut and Hohenegger, 2022; Ueyama et al., 2023) have estimated that convective moistening contributes ∼10% of the lower stratospheric H$_2$O budget, and can contribute up to ∼45% in monsoon regions (Dessler and Sherwood, 2004; Hanisco et al., 2007; Tinney and Homeyer, 2021). Ueyama et al. (2023) estimated the global inter-annual variation of lower stratospheric H$_2$O produced via deep convection between 2006 and 2016 to be on the order of a few percent (0.05-0.1 ppmv), however the time period was too short to determine any significant

trend. Further investigation is needed in order to determine if any longer-term changes in convection are influencing changes in stratospheric H_2O.

5   Conclusions

Measurements from ACE-FTS show that between 2004 and 2022 H_2O concentrations have significantly increased at a rate of approximately 1-5% dec^{-1} throughout nearly all of the stratosphere. This study uses ACE-FTS measurements of H_2O, CH_4, and N_2O, along with CMAM tropical upper-tropospheric CH_4 and ERA5 reanalysis tropical tropopause temperatures, to quantify the relative contributions of different sources of these H_2O increases. The main sources are,

- increasing tropical tropopause region temperatures. This is the main source of increasing H_2O in the tropical lower stratosphere. It accounts for H_2O increases of,

  - $\sim$2-4% dec^{-1} between 17 and 23 km in the tropics,

  - $\sim$1-2% dec^{-1} between 23 and 50 km in the tropics, and

  - $\sim$1-2% dec^{-1} 17-19 km in the mid-latitudes.

- structural BDC changes, which lead to,

  - H_2O increases of $\sim$1-2% dec^{-1} in NH mid-latitudes near 20-30 km, and

  - H_2O decreases of $\sim$1-2% dec^{-1} in SH mid-latitudes near 25-30 km and in NH mid-latitudes near 33-43 km.

- Increasing CH_4 oxidation, which causes increases in H_2O on the order of,

  - $\sim$1-2% dec^{-1} above $\sim$30 km at all latitudes and above $\sim$20 km in SH.

The solar influence on stratospheric H_2O was also investigated by regressing to F10.7 cm solar flux indicies. Its contribution to the stratospheric H_2O trends was less than 0.5% dec^{-1} in all altitude/latitude bins.

These sources combined account for all significant stratospheric H_2O trends except for a remaining $\sim$1-2% dec^{-1} increase around 30-70° latitude in both hemispheres in the mid-stratosphere ($\sim$20-35 km). These remaining trends can be accounted for by substituting the altitude-dependent CH_4 oxidation H_2O yield for a constant value of $\alpha = 3.7$ (upper limit from Wrotny et al. (2010)), possibly indicating that these increases may be due to increasing concentrations of H_2, which also oxidizes to produce H_2O.

Yet, it remains that the measured stratospheric H_2O trends currently cannot be fully explained. As time goes on and more and more satellite limb sounding missions are coming to an end, for the sake of continuity it is vital that these types of atmospheric trends are fully understood—especially if there are going to be temporal gaps between the operational periods of current and future instruments. There is an urgent need for new satellite missions to continue this observational record to enable more reliable trend estimation, as are model studies to determine what influence changes in processes such as H_2 oxidation and deep

convection—and other possible sources—are having on the stratospheric regions where the full H_2O trends cannot be fully accounted for.

References

ACE-FTS: ACE-FTS, Level 2 Data, Version 5.2, ACE-FTS [data set], https://databace.scisat.ca/level2/, last accessed: 11 Jul 2024, 2024.

Baldwin, M. P., Gray, L. J., Dunkerton, T. J., Hamilton, K., Haynes, P. H., Randel, W. J., Holton, J. R., Alexander, M. J., Hirota, I., Horinouchi, T., Jones, D. B. A., Kinnersley, J. S., Marquardt, C., Sato, K., and Takahashi, M.: The quasi-biennial oscillation, Reviews of Geophysics, 39, 179–229, https://doi.org/https://doi.org/10.1029/1999RG000073, 2001.

Beagley, S., deGrandpre, J., Koshyk, J., McFarlane, N., and Shepherd, T.: Radiative-dynamical climatology of the first-generation Canadian Middle Atmosphere Model, Atmosphere-Ocean, 35, 293–331, https://doi.org/10.1080/07055900.1997.9649595, 1997.

Bernath, P. F., McElroy, C. T., Abrams, M. C., Boone, C. D., Butler, M., Camy-Peyret, C., Carleer, M., Clerbaux, C., Coheur, P.-F., Colin, R., DeCola, P., DeMazière, M., Drummond, J. R., Dufour, D., Evans, W. F. J., Fast, H., Fussen, D., Gilbert, K., Jennings, D. E., Llewellyn, E. J., Lowe, R. P., Mahieu, E., McConnell, J. C., McHugh, M., McLeod, S. D., Michaud, R., Midwinter, C., Nassar, R., Nichitiu, F., Nowlan, C., Rinsland, C. P., Rochon, Y. J., Rowlands, N., Semeniuk, K., Simon, P., Skelton, R., Sloan, J. J., Soucy, M.-A., Strong, K., Tremblay, P., Turnbull, D., Walker, K. A., Walkty, I., Wardle, D. A., Wehrle, V., Zander, R., and Zou, J.: Atmospheric Chemistry Experiment (ACE): Mission overview, Geophysical Research Letters, 32, L15S01, https://doi.org/https://doi.org/10.1029/2005GL022386, 2005.

Boone, C., Bernath, P., Cok, D., Jones, S., and Steffen, J.: Version 4 retrievals for the Atmospheric Chemistry Experiment Fourier Transform Spectrometer (ACE-FTS) and imagers, Journal of Quantitative Spectroscopy and Radiative Transfer, 247, 106 939, https://doi.org/https://doi.org/10.1016/j.jqsrt.2020.106939, 2020.

Boone, C., Bernath, P., and Lecours, M.: Version 5 retrievals for ACE-FTS and ACE-imagers, Journal of Quantitative Spectroscopy and Radiative Transfer, 310, 108 749, https://doi.org/https://doi.org/10.1016/j.jqsrt.2023.108749, 2023.

Boone, C. D., Nassar, R., Walker, K. A., Rochon, Y., McLeod, S. D., Rinsland, C. P., and Bernath, P. F.: Retrievals for the Atmospheric Chemistry Experiment Fourier-transform spectrometer, Appl. Opt., 44, 7218–7231, https://doi.org/10.1364/AO.44.007218, 2005.

Boone, C. D., Nassar, R., Walker, K. A., Rochon, Y., McLeod, S. D., Rinsland, C. P., and Bernath, P. F.: The Atmospheric Chemistry Experiment ACE at 10: A Solar Occultation Anthology, A. Deepak Publishing, Hampton, VA, USA, 2013.

Brasseur, G. and Solomon, S.: Aeronomy of the Middle Atmosphere: Chemistry and Physics of the Stratosphere and Mesosphere, Springer, Dordrecht, 2005.

Brewer, A. W.: Evidence for a world circulation provided by the measurements of helium and water vapour distribution in the stratosphere, Quarterly Journal of the Royal Meteorological Society, 75, 351–363, https://doi.org/https://doi.org/10.1002/qj.49707532603, 1949.

Butchart, N.: The Brewer-Dobson circulation, Reviews of Geophysics, 52, 157–184, https://doi.org/https://doi.org/10.1002/2013RG000448, 2014.

Chatterjee, S. and Hadi, A. S.: Influential Observations, High Leverage Points, and Outliers in Linear Regression, Statistical Science, 1, 379–393, https://doi.org/10.1214/ss/1177013622, 1986.

Chung, E.-S., Soden, B., Sohn, B. J., and Shi, L.: Upper-tropospheric moistening in response to anthropogenic warming, Proceedings of the National Academy of Sciences, 111, 11 636–11 641, https://doi.org/10.1073/pnas.1409659111, 2014.

Dauhut, T. and Hohenegger, C.: The Contribution of Convection to the Stratospheric Water Vapor: The First Budget Using a Global Storm-Resolving Model, Journal of Geophysical Research: Atmospheres, 127, e2021JD036 295, https://doi.org/https://doi.org/10.1029/2021JD036295, e2021JD036295 2021JD036295, 2022.

Davis, S. M., Rosenlof, K. H., Hassler, B., Hurst, D. F., Read, W. G., Vömel, H., Selkirk, H., Fujiwara, M., and Damadeo, R.: The Stratospheric Water and Ozone Satellite Homogenized (SWOOSH) database: a long-term database for climate studies, Earth System Science Data, 8, 461–490, https://doi.org/10.5194/essd-8-461-2016, 2016.

400 de F. Forster, P. M. and Shine, K. P.: Stratospheric water vapour changes as a possible contributor to observed stratospheric cooling, Geophysical Research Letters, 26, 3309–3312, https://doi.org/https://doi.org/10.1029/1999GL010487, 1999.

Dee, D. P., Uppala, S. M., Simmons, A. J., Berrisford, P., Poli, P., Kobayashi, S., Andrae, U., Balmaseda, M. A., Balsamo, G., Bauer, P., Bechtold, P., Beljaars, A. C. M., van de Berg, L., Bidlot, J., Bormann, N., Delsol, C., Dragani, R., Fuentes, M., Geer, A. J., Haimberger, L., Healy, S. B., Hersbach, H., Holm, E. V., Isaksen, L., Kallberg, P., Koehler, M., Matricardi, M., McNally, A. P., Monge-Sanz,
405 B. M., Morcrette, J. J., Park, B. K., Peubey, C., de Rosnay, P., Tavolato, C., Thepaut, J. N., and Vitart, F.: The ERA-Interim reanalysis: configuration and performance of the data assimilation system, Quarterly Journal of the Royal Meteorological Society, 137, 553–597, https://doi.org/10.1002/qj.828, 2011.

Dessler, A. E. and Sherwood, S. C.: Effect of convection on the summertime extratropical lower stratosphere, Journal of Geophysical Research: Atmospheres, 109, D23 301, https://doi.org/https://doi.org/10.1029/2004JD005209, 2004.

410 Diallo, M., Legras, B., and Chédin, A.: Age of stratospheric air in the ERA-Interim, Atmospheric Chemistry and Physics, 12, 12 133–12 154, https://doi.org/10.5194/acp-12-12133-2012, 2012.

Dlugokencky, E. J., Houweling, S., Bruhwiler, L., Masarie, K. A., Lang, P. M., Miller, J. B., and Tans, P. P.: Atmospheric methane levels off: Temporary pause or a new steady-state?, Geophysical Research Letters, 30, 1992, https://doi.org/https://doi.org/10.1029/2003GL018126, 2003.

415 Dubé, K., Tegtmeier, S., Bourassa, A., Zawada, D., Degenstein, D., Sheese, P. E., Walker, K. A., and Randel, W.: N$_2$O as a regression proxy for dynamical variability in stratospheric trace gas trends, Atmospheric Chemistry and Physics, 23, 13 283–13 300, https://doi.org/https://doi.org/10.5194/acp-23-13283-2023, 2023.

Engel, A., Möbius, T., Bönisch, H., Schmidt, U., Heinz, R., Levin, I., Atlas, E., Aoki, S., Nakazawa, T., Sugawara, S., Moore, F., Hurst, D., Elkins, J., Schauffler, S., Andrews, A., and Boering, K.: Age of stratospheric air unchanged within uncertainties over the past 30 years,
420 Nature Geoscience, 2, 28–31, https://doi.org/10.1038/ngeo388, 2009.

Engel, A., Bönisch, H., Ullrich, M., Sitals, R., Membrive, O., Danis, F., and Crevoisier, C.: Mean age of stratospheric air derived from AirCore observations, Atmospheric Chemistry and Physics, 17, 6825–6838, https://doi.org/10.5194/acp-17-6825-2017, 2017.

Eyring, V., Bony, S., Meehl, G. A., Senior, C. A., Stevens, B., Stouffer, R. J., and Taylor, K. E.: Overview of the Coupled Model Intercomparison Project Phase 6 (CMIP6) experimental design and organization, Geoscientific Model Development, 9, 1937–1958,
425 https://doi.org/10.5194/gmd-9-1937-2016, 2016.

Fernando, A. M., Bernath, P. F., and Boone, C. D.: Stratospheric and mesospheric H$_2$O and CH$_4$ trends from the ACE satellite mission, Journal of Quantitative Spectroscopy and Radiative Transfer, 255, 107 268, https://doi.org/10.1016/j.jqsrt.2020.107268, 2020.

Forster, P. M. d. F. and Shine, K. P.: Assessing the climate impact of trends in stratospheric water vapor, Geophysical Research Letters, 29, 1086, https://doi.org/https://doi.org/10.1029/2001GL013909, 2002.

430 Frank, F., Jöckel, P., Gromov, S., and Dameris, M.: Investigating the yield of H$_2$O and H$_2$ from methane oxidation in the stratosphere, Atmospheric Chemistry and Physics, 18, 9955–9973, https://doi.org/10.5194/acp-18-9955-2018, 2018.

Froidevaux, L., Anderson, J., Wang, H.-J., Fuller, R. A., Schwartz, M. J., Santee, M. L., Livesey, N. J., Pumphrey, H. C., Bernath, P. F., Russell III, J. M., and McCormick, M. P.: Global OZone Chemistry And Related trace gas Data records for the Stratosphere (GOZ-

CARDS): methodology and sample results with a focus on HCl, H_2O, and O_3, Atmospheric Chemistry and Physics, 15, 10 471–10 507, https://doi.org/10.5194/acp-15-10471-2015, 2015.

Fu, Q., Solomon, S., Pahlavan, H. A., and Lin, P.: Observed changes in Brewer–Dobson circulation for 1980–2018, Environmental Research Letters, 14, 114 026, https://doi.org/10.1088/1748-9326/ab4de7, 2019.

Gelaro, R., McCarty, W., Suárez, M. J., Todling, R., Molod, A., Takacs, L., Randles, C. A., Darmenov, A., Bosilovich, M. G., Reichle, R., Wargan, K., Coy, L., Cullather, R., Draper, C., Akella, S., Buchard, V., Conaty, A., da Silva, A. M., Gu, W., Kim, G.-K., Koster, R., Lucchesi, R., Merkova, D., Nielsen, J. E., Partyka, G., Pawson, S., Putman, W., Rienecker, M., Schubert, S. D., Sienkiewicz, M., and Zhao, B.: The Modern-Era Retrospective Analysis for Research and Applications, Version 2 (MERRA-2), Journal of Climate, 30, 5419 – 5454, https://doi.org/https://doi.org/10.1175/JCLI-D-16-0758.1, 2017.

Gordon, I., Rothman, L., Hargreaves, R., Hashemi, R., Karlovets, E., Skinner, F., Conway, E., Hill, C., Kochanov, R., Tan, Y., Wcisło, P., Finenko, A., Nelson, K., Bernath, P., Birk, M., Boudon, V., Campargue, A., Chance, K., Coustenis, A., Drouin, B., Flaud, J., Gamache, R., Hodges, J., Jacquemart, D., Mlawer, E., Nikitin, A., Perevalov, V., Rotger, M., Tennyson, J., Toon, G., Tran, H., Tyuterev, V., Adkins, E., Baker, A., Barbe, A., Canè, E., Császár, A., Dudaryonok, A., Egorov, O., Fleisher, A., Fleurbaey, H., Foltynowicz, A., Furtenbacher, T., Harrison, J., Hartmann, J., Horneman, V., Huang, X., Karman, T., Karns, J., Kassi, S., Kleiner, I., Kofman, V., Kwabia–Tchana, F., Lavrentieva, N., Lee, T., Long, D., Lukashevskaya, A., Lyulin, O., Makhnev, V., Matt, W., Massie, S., Melosso, M., Mikhailenko, S., Mondelain, D., Müller, H., Naumenko, O., Perrin, A., Polyansky, O., Raddaoui, E., Raston, P., Reed, Z., Rey, M., Richard, C., Tóbiás, R., Sadiek, I., Schwenke, D., Starikova, E., Sung, K., Tamassia, F., Tashkun, S., Vander Auwera, J., Vasilenko, I., Vigasin, A., Villanueva, G., Vispoel, B., Wagner, G., Yachmenev, A., and Yurchenko, S.: The HITRAN2020 molecular spectroscopic database, Journal of Quantitative Spectroscopy and Radiative Transfer, 277, 107 949, https://doi.org/https://doi.org/10.1016/j.jqsrt.2021.107949, 2022.

Hanisco, T. F., Moyer, E. J., Weinstock, E. M., St. Clair, J. M., Sayres, D. S., Smith, J. B., Lockwood, R., Anderson, J. G., Dessler, A. E., Keutsch, F. N., Spackman, J. R., Read, W. G., and Bui, T. P.: Observations of deep convective influence on stratospheric water vapor and its isotopic composition, Geophysical Research Letters, 34, L04 814, https://doi.org/https://doi.org/10.1029/2006GL027899, 2007.

Hegglin, M. and Ye, H.: Water Vapour Climate Change Initiative (WV_cci) - CCI+ Phase 1, ATBD Part 3 - Merged CDR-3 and CDR-4 products, https://climate.esa.int/en/projects/water-vapour/key-documents/, last accessed: 23 Nov 2023, 2022.

Hegglin, M. I., Plummer, D. A., Shepherd, T. G., Scinocca, J. F., Anderson, J., Froidevaux, L., Funke, B., Hurst, D., Rozanov, A., Urban, J., von Clarmann, T., Walker, K. A., Wang, H. J., Tegtmeier, S., and Weigel, K.: Vertical structure of stratospheric water vapour trends derived from merged satellite data, Nature Geoscience, 7, 768–776, https://doi.org/10.1038/NGEO2236, 2014.

Hersbach, H., Bell, B., Berrisford, P., Hirahara, S., Horányi, A., Muñoz-Sabater, J., Nicolas, J., Peubey, C., Radu, R., Schepers, D., Simmons, A., Soci, C., Abdalla, S., Abellan, X., Balsamo, G., Bechtold, P., Biavati, G., Bidlot, J., Bonavita, M., De Chiara, G., Dahlgren, P., Dee, D., Diamantakis, M., Dragani, R., Flemming, J., Forbes, R., Fuentes, M., Geer, A., Haimberger, L., Healy, S., Hogan, R. J., Hólm, E., Janisková, M., Keeley, S., Laloyaux, P., Lopez, P., Lupu, C., Radnoti, G., de Rosnay, P., Rozum, I., Vamborg, F., Villaume, S., and Thépaut, J.-N.: The ERA5 global reanalysis, Quarterly Journal of the Royal Meteorological Society, 146, 1999–2049, https://doi.org/https://doi.org/10.1002/qj.3803, 2020.

Holton, J. R. and Gettelman, A.: Horizontal transport and the dehydration of the stratosphere, Geophysical Research Letters, 28, 2799–2802, https://doi.org/https://doi.org/10.1029/2001GL013148, 2001.

Jones, R. L., Pyle, J. A., Harries, J. E., Zavody, A. M., Russell III, J. M., and Gille, J. C.: The water vapour budget of the stratosphere studied using LIMS and SAMS satellite data, Quarterly Journal of the Royal Meteorological Society, 112, 1127–1143, https://doi.org/https://doi.org/10.1002/qj.49711247412, 1986.

Kalnay, E., Kanamitsu, M., Kistler, R., Collins, W., Deaven, D., Gandin, L., Iredell, M., Saha, S., White, G., Woollen, J., Zhu, Y., Chelliah, M., Ebisuzaki, W., Higgins, W., Janowiak, J., Mo, K. C., Ropelewski, C., Wang, J., Leetmaa, A., Reynolds, R., Jenne, R., and Joseph, D.: The NCEP/NCAR 40-Year Reanalysis Project, Bulletin of the American Meteorological Society, 77, 437 – 472, https://doi.org/10.1175/1520-0477(1996)077<0437:TNYRP>2.0.CO;2, 1996.

le Texier, H., Solomon, S., and Garcia, R. R.: The role of molecular hydrogen and methane oxidation in the water vapour budget of the stratosphere, Quarterly Journal of the Royal Meteorological Society, 114, 281–295, https://doi.org/https://doi.org/10.1002/qj.49711448002, 1988.

Manabe, S. and Wetherald, R. T.: Thermal Equilibrium of the Atmosphere with a Given Distribution of Relative Humidity, Journal of Atmospheric Sciences, 24, 241–259, https://doi.org/https://doi.org/10.1175/1520-0469(1967)024<0241:TEOTAW>2.0.CO;2, 1967.

Manney, G. L., Daffer, W. H., Zawodny, J. M., Bernath, P. F., Hoppel, K. W., Walker, K. A., Knosp, B. W., Boone, C., Remsberg, E. E., Santee, M. L., Harvey, V. L., Pawson, S., Jackson, D. R., Deaver, L., McElroy, C. T., McLinden, C. A., Drummond, J. R., Pumphrey, H. C., Lambert, A., Schwartz, M. J., Froidevaux, L., McLeod, S., Takacs, L. L., Suarez, M. J., Trepte, C. R., Cuddy, D. C., Livesey, N. J., Harwood, R. S., and Waters, J. W.: Solar occultation satellite data and derived meteorological products: Sampling issues and comparisons with Aura Microwave Limb Sounder, Journal of Geophysical Research: Atmospheres, 112, D24S50, https://doi.org/https://doi.org/10.1029/2007JD008709, 2007.

Matzka, J., Stolle, C., Yamazaki, Y., Bronkalla, O., and Morschhauser, A.: The Geomagnetic Kp Index and Derived Indices of Geomagnetic Activity, Space Weather, 19, e2020SW002 641, https://doi.org/https://doi.org/10.1029/2020SW002641, 2021.

McLandress, C., Plummer, D. A., and Shepherd, T. G.: Technical Note: A simple procedure for removing temporal discontinuities in ERA-Interim upper stratospheric temperatures for use in nudged chemistry-climate model simulations, Atmospheric Chemistry and Physics, 14, 1547–1555, https://doi.org/10.5194/acp-14-1547-2014, 2014.

Meinshausen, M., Vogel, E., Nauels, A., Lorbacher, K., Meinshausen, N., Etheridge, D. M., Fraser, P. J., Montzka, S. A., Rayner, P. J., Trudinger, C. M., Krummel, P. B., Beyerle, U., Canadell, J. G., Daniel, J. S., Enting, I. G., Law, R. M., Lunder, C. R., O'Doherty, S., Prinn, R. G., Reimann, S., Rubino, M., Velders, G. J. M., Vollmer, M. K., Wang, R. H. J., and Weiss, R.: Historical greenhouse gas concentrations for climate modelling (CMIP6), Geoscientific Model Development, 10, 2057–2116, https://doi.org/10.5194/gmd-10-2057-2017, 2017.

Meinshausen, M., Nicholls, Z. R. J., Lewis, J., Gidden, M. J., Vogel, E., Freund, M., Beyerle, U., Gessner, C., Nauels, A., Bauer, N., Canadell, J. G., Daniel, J. S., John, A., Krummel, P. B., Luderer, G., Meinshausen, N., Montzka, S. A., Rayner, P. J., Reimann, S., Smith, S. J., van den Berg, M., Velders, G. J. M., Vollmer, M. K., and Wang, R. H. J.: The shared socio-economic pathway (SSP) greenhouse gas concentrations and their extensions to 2500, Geoscientific Model Development, 13, 3571–3605, https://doi.org/10.5194/gmd-13-3571-2020, 2020.

Mote, P. W., Rosenlof, K. H., McIntyre, M. E., Carr, E. S., Gille, J. C., Holton, J. R., Kinnersley, J. S., Pumphrey, H. C., Russell III, J. M., and Waters, J. W.: An atmospheric tape recorder: The imprint of tropical tropopause temperatures on stratospheric water vapor, Journal of Geophysical Research: Atmospheres, 101, 3989–4006, https://doi.org/https://doi.org/10.1029/95JD03422, 1996.

Myhre, G., Nilsen, J. S., Gulstad, L., Shine, K. P., Rognerud, B., and Isaksen, I. S. A.: Radiative forcing due to stratospheric water vapour from CH_4 oxidation, Geophysical Research Letters, 34, L01 807, https://doi.org/https://doi.org/10.1029/2006GL027472, 2007.

Polvani, L. M., Abalos, M., Garcia, R., Kinnison, D., and Randel, W. J.: Significant Weakening of Brewer-Dobson Circulation Trends Over the 21st Century as a Consequence of the Montreal Protocol, Geophysical Research Letters, 45, 401–409, https://doi.org/https://doi.org/10.1002/2017GL075345, 2018.

Poshyvailo-Strube, L., Müller, R., Fueglistaler, S., Hegglin, M. I., Laube, J. C., Volk, C. M., and Ploeger, F.: How can Brewer–Dobson
circulation trends be estimated from changes in stratospheric water vapour and methane?, Atmospheric Chemistry and Physics, 22, 9895–
9914, https://doi.org/10.5194/acp-22-9895-2022, 2022.

Randel, W. and Park, M.: Diagnosing Observed Stratospheric Water Vapor Relationships to the Cold Point Tropical Tropopause, Journal of
Geophysical Research: Atmospheres, 124, 7018–7033, https://doi.org/https://doi.org/10.1029/2019JD030648, 2019.

Rigby, M., Prinn, R. G., Fraser, P. J., Simmonds, P. G., Langenfelds, R. L., Huang, J., Cunnold, D. M., Steele, L. P., Krummel, P. B., Weiss,
R. F., O'Doherty, S., Salameh, P. K., Wang, H. J., Harth, C. M., Mühle, J., and Porter, L. W.: Renewed growth of atmospheric methane,
Geophysical Research Letters, 35, L22 805, https://doi.org/https://doi.org/10.1029/2008GL036037, 2008.

Rong, P., Russell, J. M., Marshall, B. T., Gordley, L. L., Mlynczak, M. G., and Walker, K. A.: Validation of water va-
por measured by SABER on the TIMED satellite, Journal of Atmospheric and Solar-Terrestrial Physics, 194, 105 099,
https://doi.org/https://doi.org/10.1016/j.jastp.2019.105099, 2019.

Scinocca, J. F., McFarlane, N. A., Lazare, M., Li, J., and Plummer, D.: Technical Note: The CCCma third generation AGCM and its extension
into the middle atmosphere, Atmospheric Chemistry and Physics, 8, 7055–7074, https://doi.org/10.5194/acp-8-7055-2008, 2008.

Sheese, P. E. and Walker, K. A.: Data Quality Flags for ACE-FTS Level 2 Version 5.2 Data Set, Borealis, V14 [data set],
https://doi.org/https://doi.org/10.5683/SP3/NAYNFE, borealis, V14, 2024, 2024.

Sheese, P. E., Boone, C. D., and Walker, K. A.: Detecting physically unrealistic outliers in ACE-FTS atmospheric measurements, Atmo-
spheric Measurement Techniques, 8, 741–750, https://doi.org/10.5194/amt-8-741-2015, 2015.

Stowasser, M., Oelhaf, H., Wetzel, G., Friedl-Vallon, F., Maucher, G., Seefeldner, M., Trieschmann, O., v. Clarmann, T., and Fischer, H.:
Simultaneous measurements of HDO, H_2O, and CH_4 with MIPAS-B: Hydrogen budget and indication of dehydration inside the polar
vortex, Journal of Geophysical Research: Atmospheres, 104, 19 213–19 225, https://doi.org/https://doi.org/10.1029/1999JD900239, 1999.

Tao, M., Konopka, P., Wright, J. S., Liu, Y., Bian, J., Davis, S. M., Jia, Y., and Ploeger, F.: Multi-decadal variability controls short-term
stratospheric water vapor trends, Communications Earth and Environment, 4, 441, https://doi.org/10.1038/s43247-023-01094-9, 2023.

Tinney, E. N. and Homeyer, C. R.: A 13-year Trajectory-Based Analysis of Convection-Driven Changes in Upper Troposphere
Lower Stratosphere Composition Over the United States, Journal of Geophysical Research: Atmospheres, 126, e2020JD033 657,
https://doi.org/https://doi.org/10.1029/2020JD033657, 2021.

Ueyama, R., Schoeberl, M., Jensen, E., Pfister, L., Park, M., and Ryoo, J.-M.: Convective Impact on the Global Lower Stratospheric Water Va-
por Budget, Journal of Geophysical Research: Atmospheres, 128, e2022JD037 135, https://doi.org/https://doi.org/10.1029/2022JD037135,
2023.

Weaver, D., Strong, K., Walker, K. A., Sioris, C., Schneider, M., McElroy, C. T., Vömel, H., Sommer, M., Weigel, K., Rozanov, A., Burrows,
J. P., Read, W. G., Fishbein, E., and Stiller, G.: Comparison of ground-based and satellite measurements of water vapour vertical profiles
over Ellesmere Island, Nunavut, Atmospheric Measurement Techniques, 12, 4039–4063, https://doi.org/10.5194/amt-12-4039-2019, 2019.

Wetzel, G., Oelhaf, H., Berthet, G., Bracher, A., Cornacchia, C., Feist, D. G., Fischer, H., Fix, A., Iarlori, M., Kleinert, A., Lengel, A., Milz,
M., Mona, L., Müller, S. C., Ovarlez, J., Pappalardo, G., Piccolo, C., Raspollini, P., Renard, J.-B., Rizi, V., Rohs, S., Schiller, C., Stiller,
G., Weber, M., and Zhang, G.: Validation of MIPAS-ENVISAT H_2O operational data collected between July 2002 and March 2004,
Atmospheric Chemistry and Physics, 13, 5791–5811, https://doi.org/10.5194/acp-13-5791-2013, 2013.

Wolter, K. and Timlin, M. S.: El Niño/Southern Oscillation behaviour since 1871 as diagnosed in an extended multivariate ENSO index
(MEI.ext), International Journal of Climatology, 31, 1074–1087, https://doi.org/https://doi.org/10.1002/joc.2336, 2011.

Wrotny, J. E., Nedoluha, G. E., Boone, C., Stiller, G. P., and McCormack, J. P.: Total hydrogen budget of the equatorial upper stratosphere, Journal of Geophysical Research: Atmospheres, 115, D04 302, https://doi.org/https://doi.org/10.1029/2009JD012135, 2010.

Ye, H., Hegglin, M., Schröder, M., and Niedor, A.: Water Vapour Climate Change Initiative (WV_cci) - CCI+ Phase 1, Product Validation and Intercomparison Report (PVIR) - Part 2: CDR-3 & CDR-4, https://climate.esa.int/en/projects/water-vapour/key-documents/, last accessed: 23 Nov 2023, 2022.

Yue, J., Russell III, J., Gan, Q., Wang, T., Rong, P., Garcia, R., and Mlynczak, M.: Increasing Water Vapor in the Stratosphere and Mesosphere After 2002, Geophysical Research Letters, 46, 13 452–13 460, https://doi.org/https://doi.org/10.1029/2019GL084973, 2019.

550
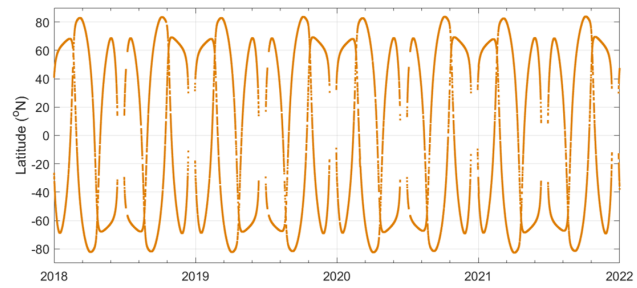
Figure 1. Latitudinal coverage of the ACE-FTS measurements for 2018-2022.
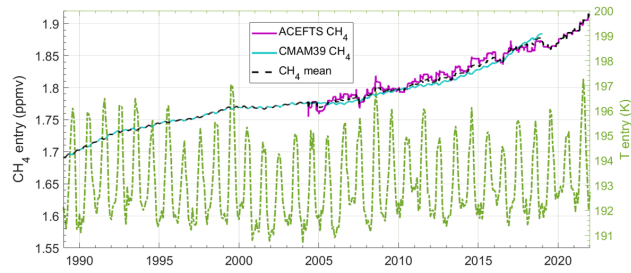
Figure 2. Mean CH$_4$ time series for 15°S-15°N and 100-200 hPa. ACE-FTS data (cyan) are 180-day running means and the CMAM39 data (magenta) are daily means. The mean of ACE-FTS and CMAM39 (black dashes) was used to determine the CH$_4$ entry trend. Also, ERA5 temperatures (green dot-dash) are monthly mean values for 15°S-15°N at 100 hPa.
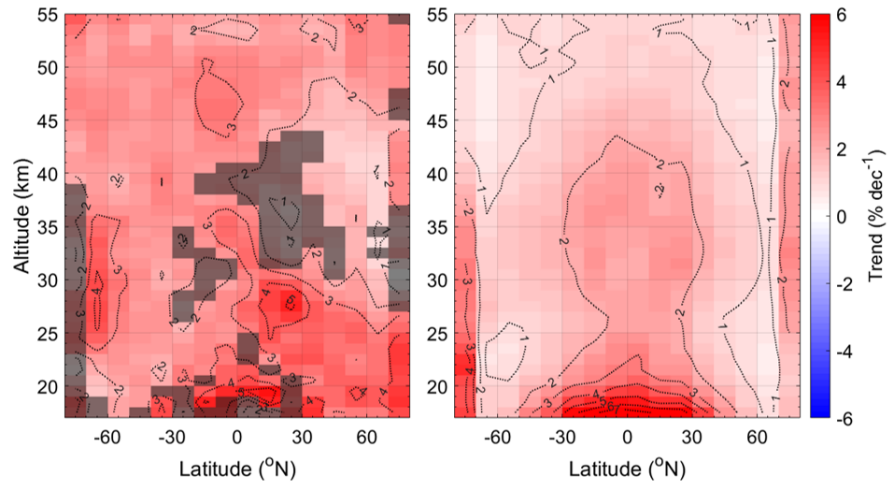
Figure 3. ACE-FTS H$_2$O trends. (left) Full trends (where only regressing to ~~linear components and~~ semi-annual and annual cycles) and (right) corresponding trend uncertainty to a confidence level of 95%. Shaded regions in left panel indicate regions with no significant trend to within 95%.
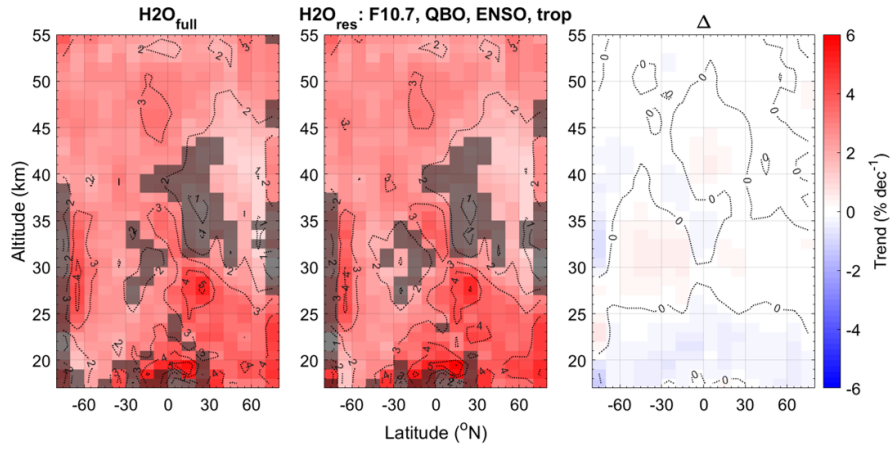
Figure 4. ACE-FTS H_2O trends. (left) Full trends (where only regressing to ~~linear components and~~ semi-annual and annual cycles). (middle) Residual H_2O trends after regressing to F10.7 cm, QBO, ENSO, and tropopause pressure time series and semi-annual and annual cycles. (right) The difference between the full trends and the residual trends. Shaded regions in left and middle panels indicate regions with no significant trend to within 95%.
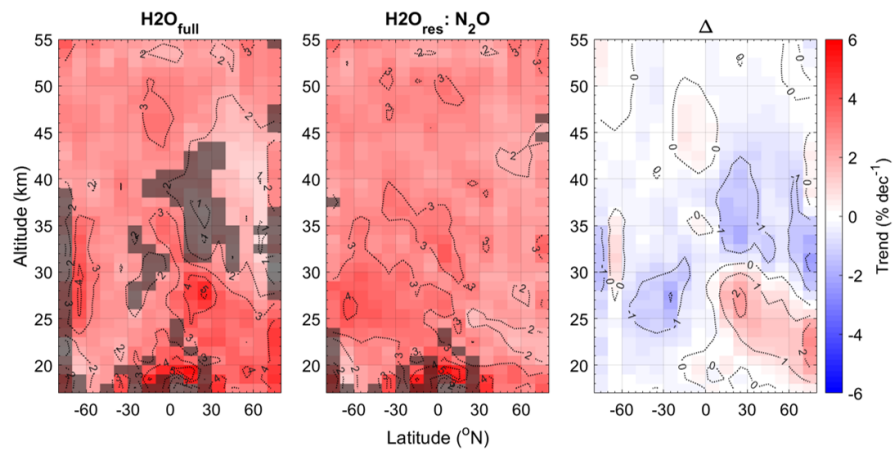
Figure 5. Same as Fig. 4, except the residual H_2O trends (middle) are after regressing to N_2O and semi-annual and annual cycles.
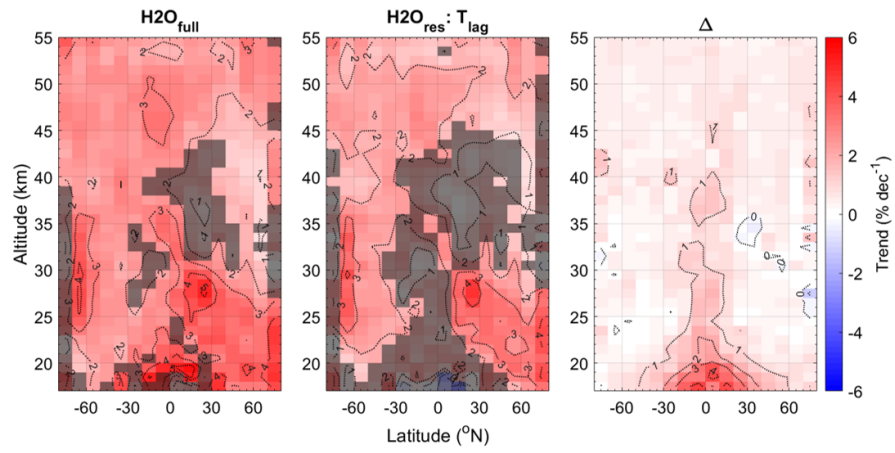
Figure 6. Same as Fig. 4, except the residual H$_2$O trends (middle) are after regressing to ERA5 temperatures with empirically determined time lags (T_{lag}) and semi-annual and annual cycles.
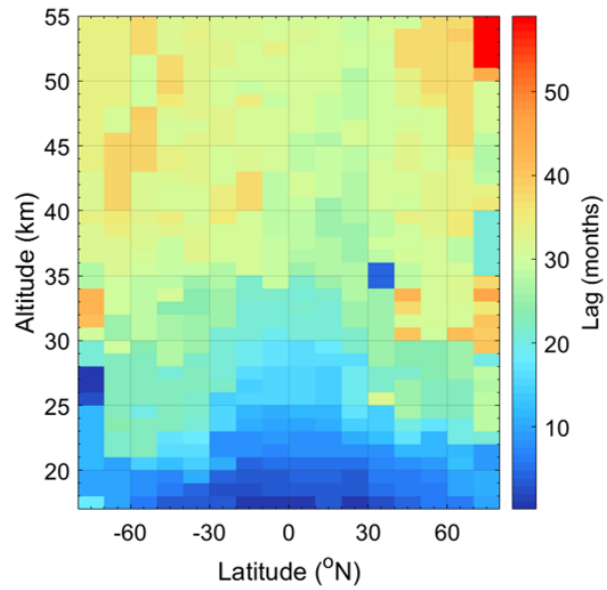
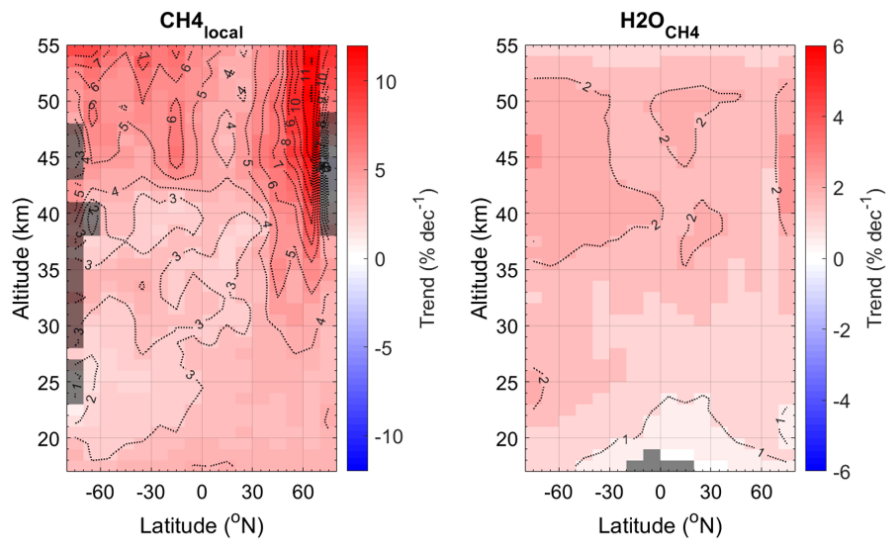**Figure 7.** Lag times introduced to the ERA5 temperature time series (T_{lag}) that minimize the residuals between the ACE-FTS data and the MLR fit.

Figure 8. (left) ACE-FTS CH_4 local trends and (right) contribution of CH_4 oxidation to ACE-FTS H_2O trends. Shaded regions indicate regions with no significant trend to within 95%.
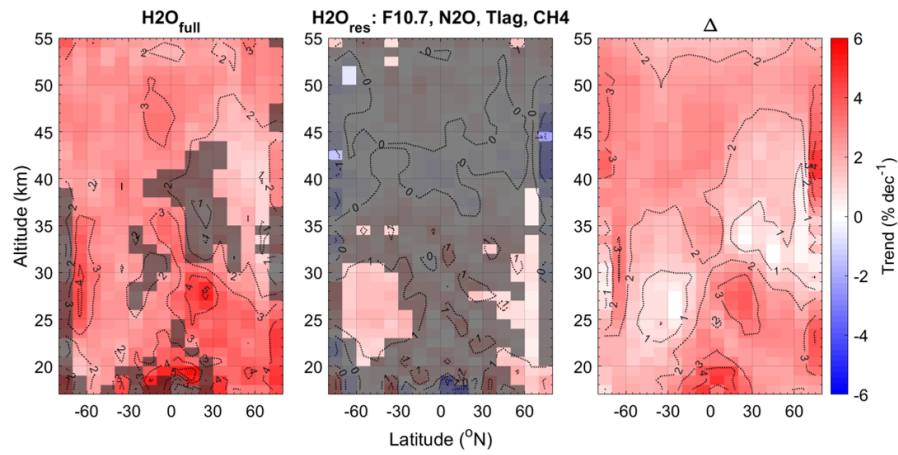
Figure 9. Same as Fig. 4, except the residual H_2O trends (middle) are after regressing to semi-annual and annual cycles, F10.7 cm flux, N_2O, T_{lag} time series and accounting for CH_4 oxidation.
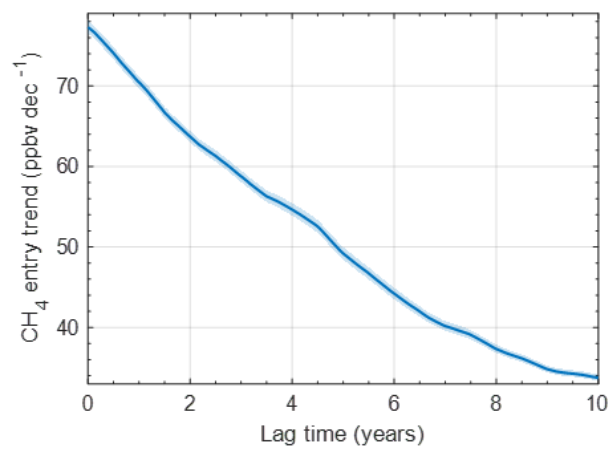
Figure 10. 18-year CH₄ entry trends, as a function of lag time, for time periods of 1994-2012 (lag of 10 years) to 2004-2022 (lag of 0 years). Shaded region represents the 95% confidence levels.
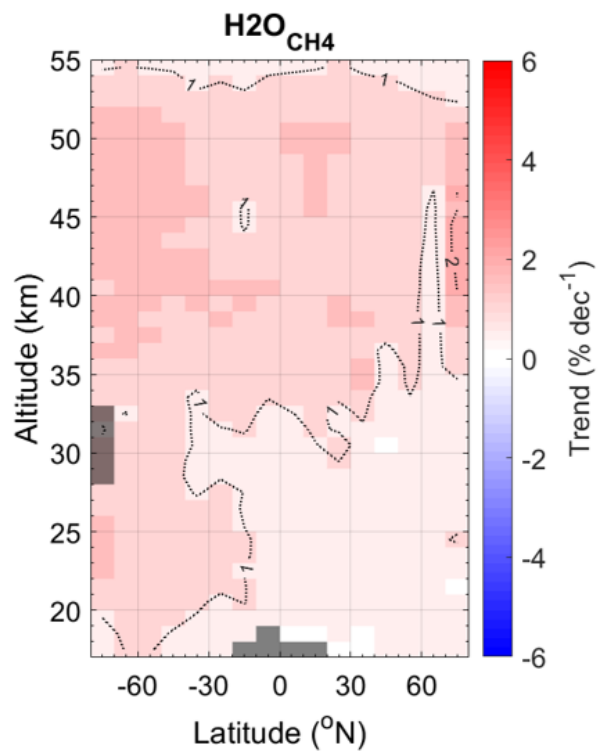
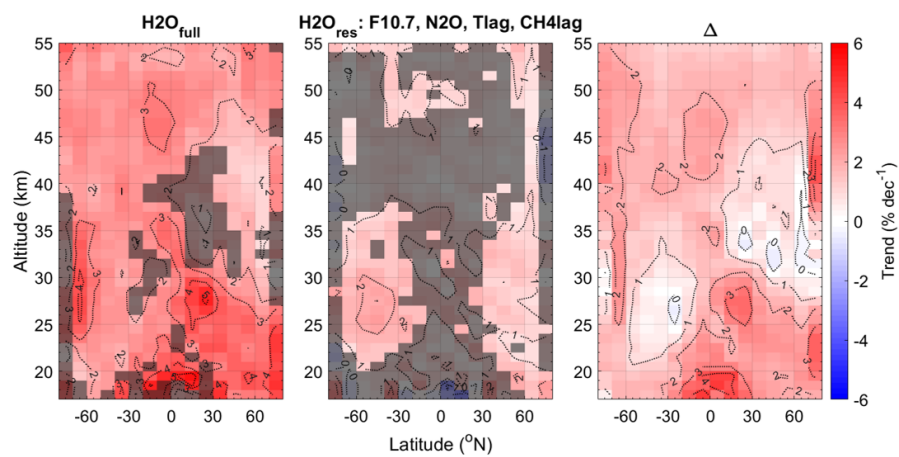**Figure 11.** Trends in H_2O due to CH_4 oxidation using time-lagged CH_4 entry trend values (based on T_{lag} lag times).

Figure 12. Same as Fig. 9 except time-lagged CH$_4$ entry trend values (based on T_{lag} lag times) were used when accounting for CH$_4$ oxidation.
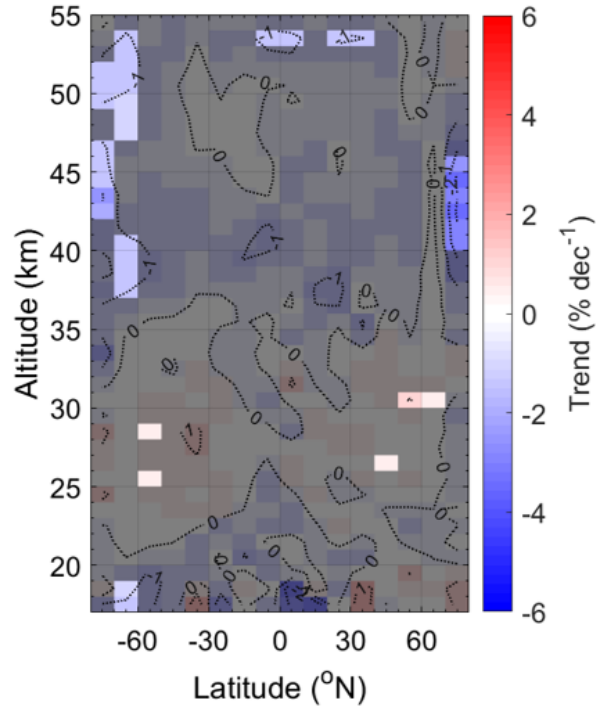
Figure 13. ~~Trends in~~ Residual H_2O ~~due~~ trends after regressing to semi-annual and annual cycles, F10.7 cm flux, N_2O, T_{lag} time series and accounting for CH_4 oxidation using time-lagged CH_4 entry ~~trend~~ values ~~(based on T_{lag} lag times)~~ and a H_2O yield value of $\alpha = 3.7$ in all altitude/latitude bins. Shaded regions indicate regions with no significant trend to within 95%.

Appendix A

A1 Time lagged ENSO and tropopause pressure

555   The effects of ENSO conditions and tropopause pressure on stratospheric H_2O, however, are not instantaneous. Similar to the time-lagging method described in Sect. 3, the ENSO and trop time series were lagged to find lag times in each bin that maximize the correlations between local H_2O and the respective index time series. The influence of lagged ENSO and lagged trop on H_2O trends are shown in the top panel of Fig. A1 and the respective corresponding optimal lag times in months are shown on the bottom. The influence of both lagged ENSO and lagged trop is still typically less than 1% dec^{-1} throughout the

560   stratosphere.

A2 Correlation with AO

When accounting for CH_4 oxidation with time-lagged entry trends and regressing to T_{lag} and N_2O and SAO and no AO components, the resulting residual trends are not meaningfully different below ~42 km from the same case with AO as a regressor, as seen in Fig. A2. The main differences are above 42 km. Without including AO, the region with significant residual

565   trends in the low-mid latitudes is larger, but still on the order of 1% $dec-1$, the SH high latitudes exhibit negative residual trends on the order of -1% dec^{-1}, and the NH mid-high latitudes exhibit no significant trends. Therefore, further study is still needed to fully parse the H_2O trends in the upper stratosphere.
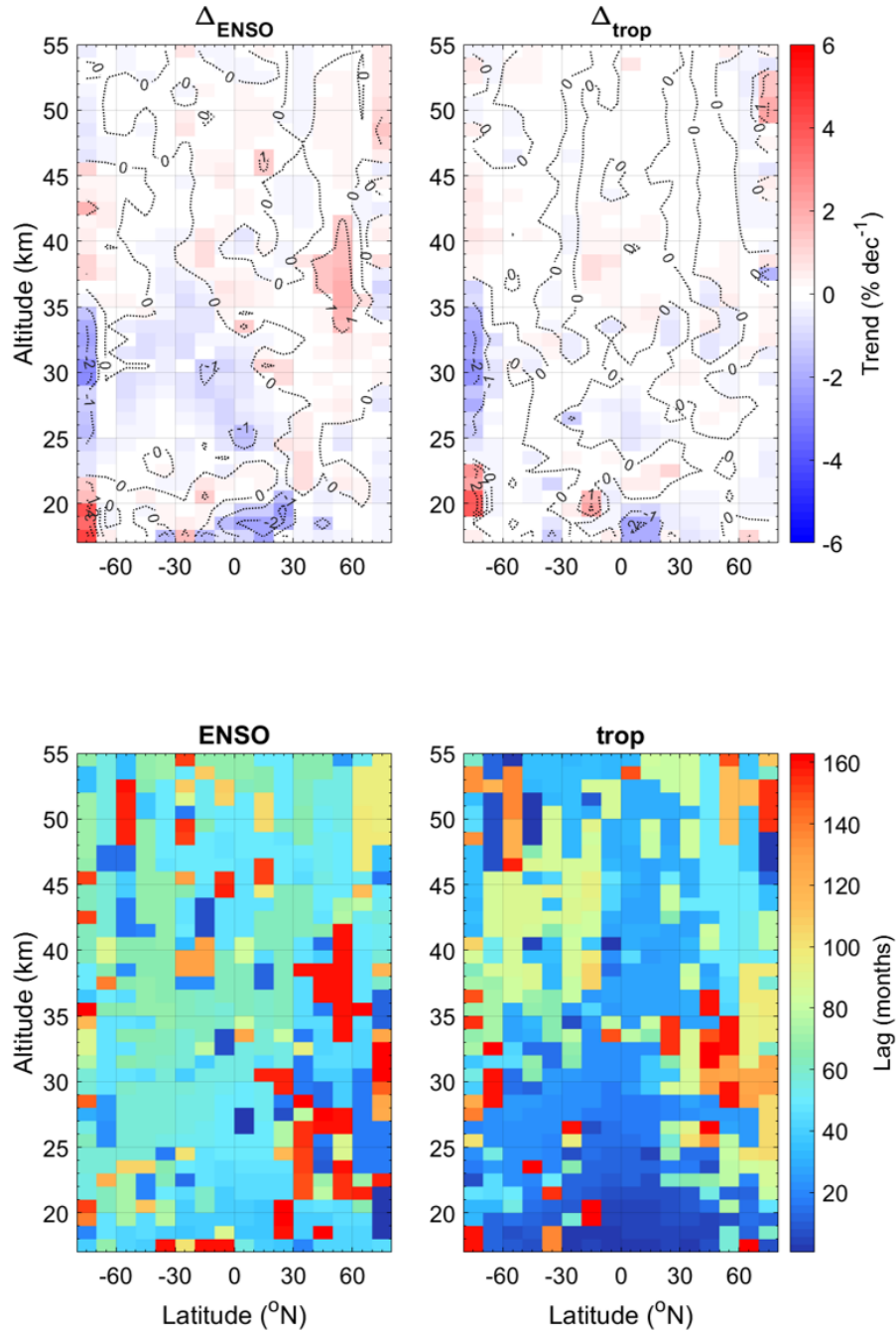
Figure A1. (top) The difference between the full trends and the residual trends when regressing to the lagged ENSO (left) and trop (right) time series and semi-annual and annual cycles. (bottom) The corresponding optimal lag times.
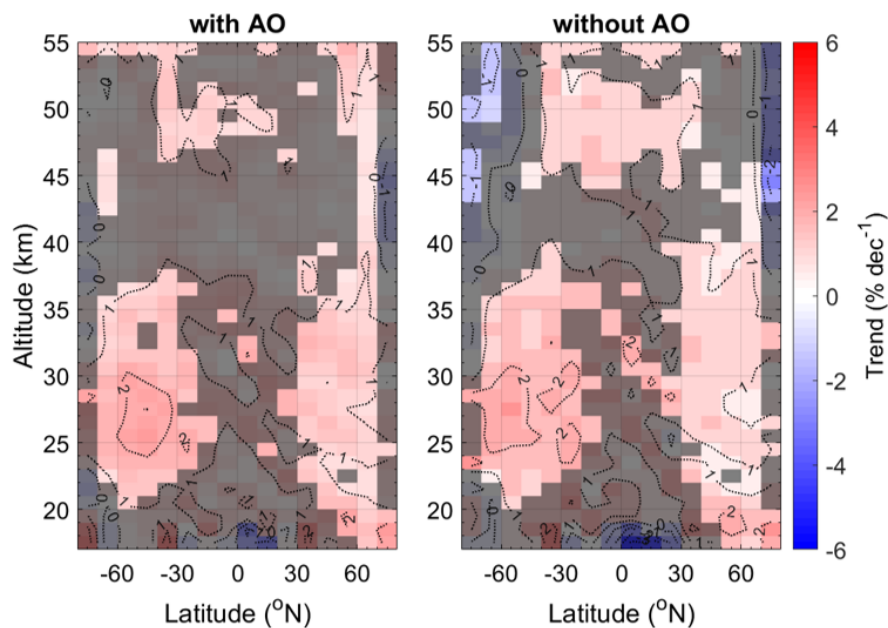
Figure A2. (left) Residual H_2O trends after regressing to semi-annual and annual cycles, F10.7 cm flux, N_2O, T_{lag} time series and accounting for CH_4 oxidation using time-lagged CH_4 entry values. (right) Same as (left) but without regressing to annual cycles. Shaded regions indicate regions with no significant trend to within 95%.

~~Residual H_2O trends after regressing to semi-annual and annual cycles, F10.7 cm flux, N_2O, T_{lag} time series and accounting for CH_4 oxidation using time-lagged CH_4 entry values and a H_2O yield value of $\alpha = 3.7$ in all altitude/latitude bins. Shaded regions indicate regions with no significant trend to within 95%.~~

570